JACS
JOURNAL OF THE AMERICAN CHEMICAL SOCIETY
Article
pubs.acs.org/JACS

Impact of Diradical Character on Two-Photon Absorption: Bis(acridine) Dimers Synthesized from an Allenic Precursor

Kenji Kamada,*[,†] Shin-ichi Fuku-en,[‡] Shu Minamide,[†,§] Koji Ohta,[†] Ryohei Kishi,[§] Masayoshi Nakano,[§] Hiroyuki Matsuzaki,[∥,⊥] Hiroshi Okamoto,[∥] Hiroyuki Higashikawa,[‡] Katsuya Inoue,[‡] Satoshi Kojima,[‡] and Yohsuke Yamamoto*[,‡]

[†]Research Institute for Ubiquitous Energy Devices, National Institute of Advanced Industrial Science and Technology (AIST), Ikeda, Osaka 563-8577, Japan

[‡]Department of Chemistry, Graduate School of Science, Hiroshima University, 1-3-1 Kagamiyama, Higashi-Hiroshima 739-8526, Japan

[§]Department of Materials Engineering Science, Graduate School of Engineering Science, Osaka University, Toyonaka, Osaka 560-8531, Japan

[∥]Department of Advanced Material Science, Graduate School of Frontier Sciences, University of Tokyo, Kashiwa, Chiba 277-8561, Japan

Supporting Information

ABSTRACT: The two-photon absorption (TPA) of a bis(acridine) dimer (**8**) having singlet diradical character in its ground state was found to be enhanced by more than 2 orders of magnitude as compared to its closed-shell counterpart (**12**), which has the same structural backbone and atom composition. The dimer, a tetracation species consisting of two connected acridinium cation moieties with high coplanarity, was obtained during our attempts to synthesize triplet carbenes by double oxidation of an allenic precursor (**3b**). High conjugation over the two aromatic rings connected by dimerization was revealed by X-ray analysis, and a small HOMO−LUMO gap was found in the visible-near-infrared one-photon absorption spectrum in solution and in the crystalline state, exhibiting that the ground state of **8** has singlet diradical nature. Ab initio molecular orbital calculations of the ground state also suggested that **8** has an intermediate diradical character (y) of 0.685. Interconversion between diradical tetracation dimer **8** and closed-shell dication dimer **12** was achieved by oxidation/reduction in good yields and was accompanied by formation of monoradical trication dimer **13** as an intermediate. TPA measurements at near-infrared wavelengths revealed that diradical dimer **8** has large TPA cross sections (3600 GM at 1200 nm), while closed-shell **12** has TPA cross sections of <21 GM. This result represents a straightforward comparison between the TPA activity of molecules with the same structural backbone and atom composition but with different degree of the diradical character, supporting the theoretical prediction that enhanced TPA intensity can be observed in the intermediate y region ($0 < y < 1$).

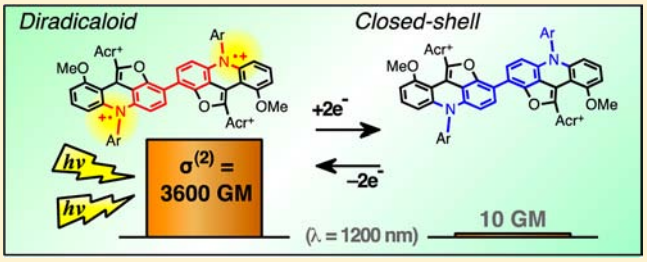

1. INTRODUCTION

The concept of singlet diradicals is key to understanding the nature of chemical bonds; thus, their electronic properties have been investigated extensively.[1] However, it has only been several years since the singlet diradical nature of aromatic hydrocarbons has attracted considerable attention because of extensive progress in their theory, synthesis, and functionality.[2] Prediction of the diradical nature of oligoacenes by Bendikov et al.[3] stimulated further theoretical[4] and synthetic[5] studies of oligoacenes with longer π-conjugation. Thermodynamic stabilization of the singlet diradical state was realized by Kubo et al. through studies of the bis(phenalenyl) structure.[6] The bis(phenalenyl) diradicaloids have significant singlet diradical nature and exhibit the coexistence of intra- and intermolecular covalent bonds originating from the open-shell character.[6,7]

Clearly, molecules with partial singlet diradical nature in their ground state, that is, singlet diradicaloids, are expected to have interesting physical properties (electronic, optical, magnetic, etc.) in addition to their structural uniqueness. Indeed, a remarkable enhancement of the molecular third-order nonlinear optical (NLO) property, that is, second hyperpolarizability (γ), was theoretically predicted in the intermediate bond breaking region with partial singlet diradical character for the H_2 molecule.[8] The ground-state electronic structure of singlet diradicaloids is characterized by the diradical character, y, which

Received: August 30, 2012
Published: December 6, 2012

 © 2012 American Chemical Society

is defined by the occupation number of the lowest unoccupied natural orbital (LUNO) having antibonding nature. The y value therefore represents the "degree" of the singlet diradical character, that is, bond weakness (y = 0 for the closed-shell and y = 1 for pure singlet diradicals), so that, in other words, 1 − y indicates an "effective bond order". The theoretical assessments of γ for singlet diradicaloid model molecules[9a,b] revealed that γ has a bell-shape dependence as a function of the diradical character y. This relationship has been theoretically proven on the basis of the valence configuration interaction two-site model[9c,d] not only in static γ but also in two-photon absorption (TPA) cross section, which is the molecular quantity proportional to the imaginary part of γ and an important property for various potential applications.[10] This can be qualitatively understood by the perturbative formula of $\gamma \approx (\mu_{g,e1})^2(\mu_{e1,e2})^2/(E_{e1})^2(E_{e2})$,[9b,c] as well as by the y dependences of excitation energies (E_{e1}, E_{e2}) and transition moments ($\mu_{g,e1}$, $\mu_{e1,e2}$) concerning the ground (g) and low-lying excited states (e1, e2); that is, the increase in the y leads to the decrease of $\mu_{g,e1}$ and E_n, while to the increase of $\mu_{e1,e2}$. The relationship has also been exemplified using ab initio MO and density functional theory calculations for model and real molecular systems, for example, polycyclic aromatic hydrocarbons including thermally stable bis(phenalenyl) systems,[11a] graphene nanoflakes,[11b] and transition-metal systems.[11c] Originally, y is defined in a purely theoretical manner;[12] however, the analytical formula to estimate the y value from experimentally accessible quantities was proposed to fill the gap between theoretical predictions and experimental observations obtained from one- and two-photon absorption spectra as well as from phosphorescence and electron spin resonance peaks.[13] Experimental results revealed that bis(phenalenyl)-based diradicaloids have the TPA cross sections of 1 or 2 orders of magnitude larger than those of aromatic hydrocarbons that have similar π-conjugation length, but less diradical character.[14] However, such comparisons have left ambiguities because the structures of the diradicaloid and closed-shell molecules are not the same.

During our attempts to synthesize stable triplet carbenes for other purposes, we serendipitously obtained a series of compounds having different levels of singlet diradical character with the same structural backbone. The previous approach for preparing triplet carbenes was photolysis of diazo compound **1** to generate the relatively persistent triplet carbene **2** (Scheme 1).[15,16] As structural elucidation of **2** in a pure state has not been achieved,[17] we tried a new strategy based on the two-electron oxidation of allenic precursors (Scheme 2). We tested the chemical oxidation of allenic compounds **3a**, **3b**, and **5**, but did not observe any triplet carbenes. However, we found that the oxidation of allene **3b** gave rise to tetracation **8**, an unexpected product having partial singlet diradical character, through demethylation and dimerization (Figure 1).[18,19] Dimer **8** can have the resonance structures **8A**, the closed-shell quinoid, and diradical nonquinoidal form **8B**, similar to the case of Chichibabin's hydrocarbon,[20] a widely known example of a diradicaloid (Figure 2). Moreover, chemical reduction of **8** gave monoradical and closed-shell compounds with tricationic and dicationic charges, respectively. This means that the redox reaction can change the diradical character of the molecules without changing the structural backbone. This property is ideal for studying the relationship between the TPA property and diradical character by direct comparison.

Scheme 1. Reported Method for the Synthesis of the Most Persistent Triplet Carbene Known

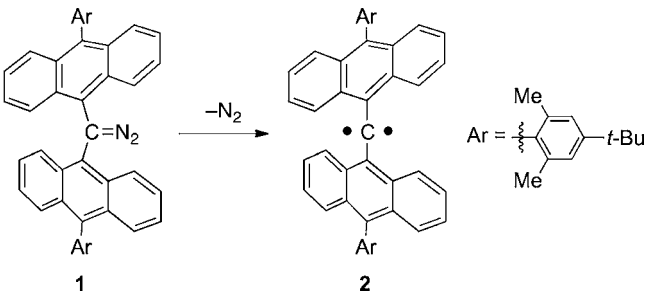

In this Article, we report on the synthesis, diradical nature, and TPA properties of dimer **8** and its closed-shell (**12**) and monoradical (**13**) counterparts. The diradical nature of dimer **8** is discussed on the basis of X-ray structural analysis, one-photon absorption measurements, and theoretical calculations. These results support that **8** has significant diradical nature with an intermediate magnitude of y = 0.685. TPA measurements by the femtosecond Z-scan method revealed that diradical dimer **8** has intense TPA (maximum TPA cross section $\sigma^{(2)}$ = 3600 GM at 1200 nm, where 1 GM = 10^{-50} cm^4 s molecule^{-1} photon^{-1}). On the other hand, the $\sigma^{(2)}$ of closed-shell counterpart **12** was less than 20 GM. This high contrast in the value of $\sigma^{(2)}$ by more than 2 orders of magnitudes, resulting from the change in the value of y, clearly supports the theoretical prediction of enhancement of $\sigma^{(2)}$ with intermediate diradical character y. This is the first direct comparison, to the best of our knowledge, between a singlet diradicaloid (**8**, y = 0.682) and its closed-shell counterpart (**12**, y = 0.000), which have the same backbone structure and atom composition (but different charged state), although comparisons between molecules having similar π-conjugation (but different backbones or atom compositions) have been previously demonstrated.[13,14,21] It is here noted that the introduction of positive charges tends to mainly affect the contribution of type II virtual excitation process (negative) to γ,[22] while the enhancement of γ in the intermediate diradical character region is found to be primarily caused by that of type III (positive) process.[9b,c] Thus, such differences in charged states are not predicted to provide a strong influence on the diradical character dependences of γ in the present compounds.

The syntheses of diradical dimer **8** and its precursors are presented in sections 2.1 and 2.2, followed by the evaluation of the diradical nature of **8** in section 2.3. Derivation of its closed-shell counterpart **12** and monoradical species **13** is described in section 2.4, and plausible mechanisms of the reactions are discussed in section 2.5. The one- and two-photon absorption properties of **8**, **12**, and **13** are presented in sections 2.6 and 2.7, respectively. The conclusions are given in section 3. The synthetic, experimental, and calculation procedures are presented in the Supporting Information.

2. RESULTS AND DISCUSSION

2.1. Synthesis of Allenic Precursor 3b. The allenic precursor (**3b**) was prepared as shown in Scheme 3. The key intermediate, acridone **10**, was synthesized by a procedure similar to that described previously.[23] The methoxy-substituted triarylamine (**9**) was synthesized by the Buchwald−Hartwig cross-coupling reaction.[24] Selective dilithiation of amine **9** upon reaction with n-BuLi in refluxing n-hexane, followed by treatment with methyl chloroformate, afforded the desired

Scheme 2. Our Strategy To Generate Stable Triplet Carbenes

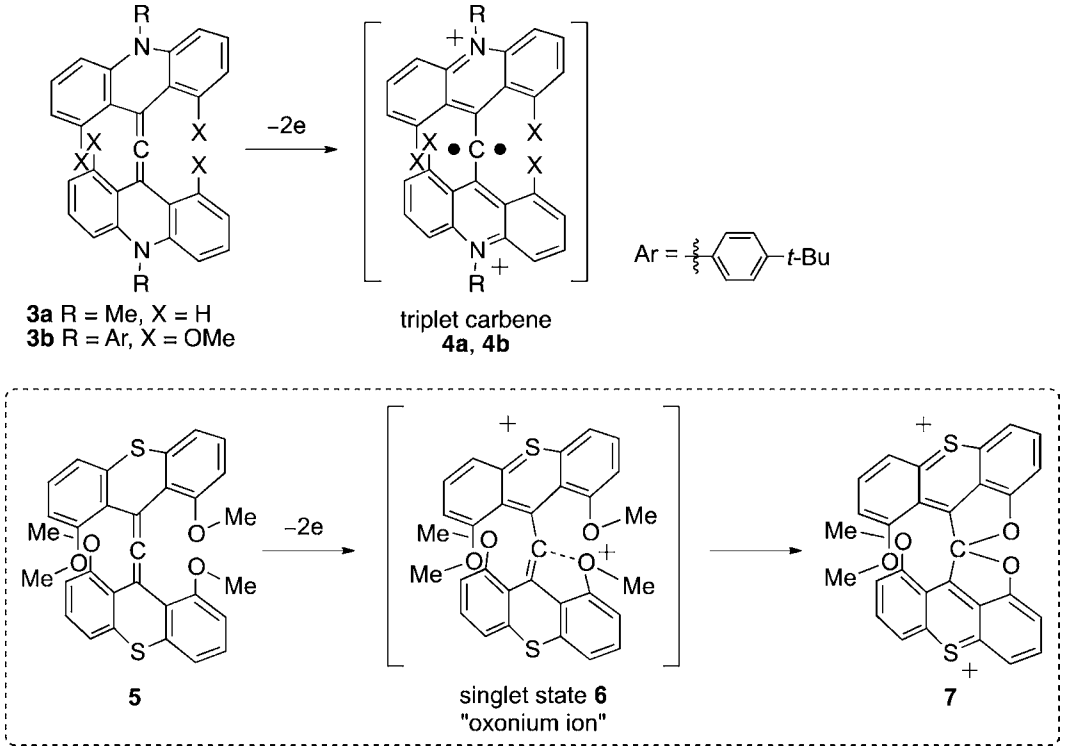

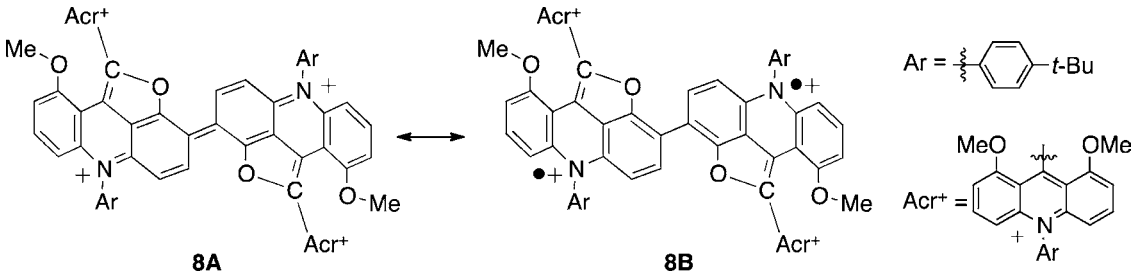

Figure 1. Isolated dimeric species **8**.

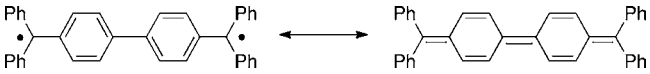

Figure 2. Chichibabin's hydrocarbon.

Scheme 3. Synthesis of Allenic Precursor 3b

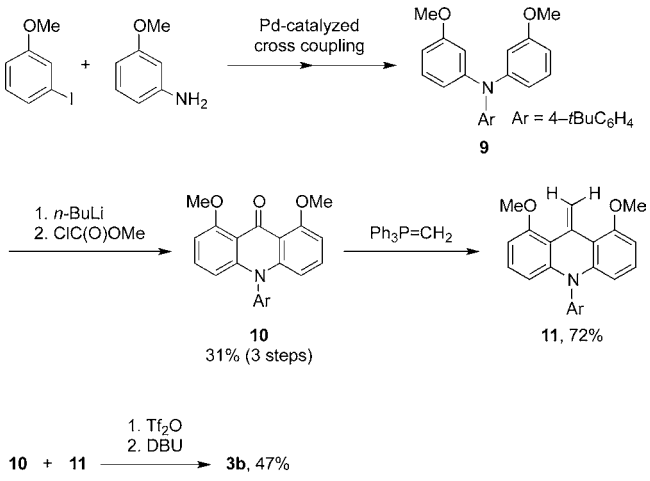

acridone **10** in 31% over three steps. Acridone **10** was easily converted to the corresponding olefin **11** by the Wittig reaction. The reaction[25] of acridone **10** with olefin **11** in the presence of Tf_2O followed by treatment with DBU afforded the desired allene **3b** in 47% yield. Compound **3b** showed a signal characteristic of allenic carbons in the ^{13}C NMR spectrum at 216.2 ppm. X-ray analysis confirmed the structure and revealed the presence of a bent allene framework with an angle of 168.0(2)°, which must have resulted from steric crowding caused by the two acridine units (Figure 3).

2.2. Oxidation of Allenic Precursor and Crystal Structure of Isolated Dimer Species. The oxidation of **3b** with 2 equiv of $(4\text{-}BrC_6H_4)_3N^{\bullet+}SbCl_6^-$ in CH_2Cl_2 afforded a dark purple solid. X-ray analysis of single crystals obtained by recrystallization from CH_3CN/ether revealed the compound to be **8**·$4SbCl_4$. It can be rationalized that this compound resulted from demethylation and dimerization of the reactant allene **3b** (Figure 4).[26] A small amount of impurity that was later revealed by UV−vis−NIR measurements to be trication monoradical **13**, resulting from incomplete oxidation, also formed and could not be removed fully from **8**·$4SbCl_4$, even upon recrystallization. Probably because of the presence of this species, which is capable of undergoing rapid electron transfer with **8**·$4SbCl_4$, the

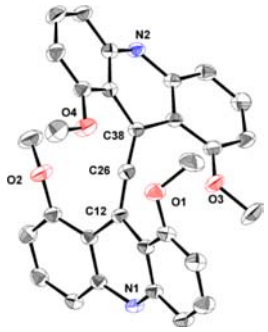

Figure 3. Molecular structure of **3b**. Hydrogen atoms, 4-*t*-BuC_6H_4 groups, and incorporated solvent molecules have been omitted for clarity. Thermal ellipsoids are drawn at the 50% probability level. Selected bond lengths [Å] and angles [deg] for **3b**: C12−C26 = 1.311(4), C26−C38 = 1.317(3), C12−C26−C38 = 168.0(2).

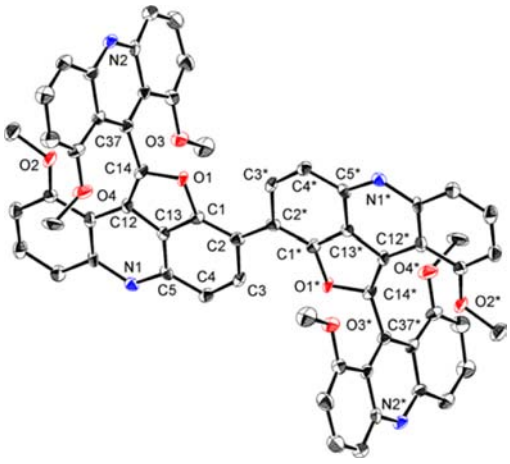

Figure 4. Molecular structure of **8**·4$SbCl_4$. Hydrogen atoms, 4-*t*-BuC_6H_4 groups, counteranions, and incorporated solvent molecules have been omitted for clarity. Thermal ellipsoids are drawn at the 50% probability level. Selected bond lengths [Å] and angles [def] for **8**·4$SbCl_4$: N1−C5 = 1.336(10), C1−C2 = 1.405(12), C2−C3 = 1.441(12), C3−C4 = 1.379(10), C4−C5 = 1.410(12), C5−C13 = 1.411(12), C13−C1 = 1.366(10), C2−C2* = 1.420(10), C1−C2−C2*−C3* = 0.19(12), C12−C14 = 1.374(12), C14−C37 = 1.516(12), C12−C14−C37 = 137.4(4).

NMR spectrum was extensively broadened. A radical impurity was detected by measuring the ESR spectrum of crude **8**·4$SbCl_4$ (see the Supporting Information). Nonetheless, the single crystals obtained were sufficient for X-ray structural analysis. In the hope that pure samples might be obtained, counteranion exchange of $SbCl_4^-$ with $CHB_{11}H_5Cl_6^-$ was carried out to furnish **8**·4$CHB_{11}H_5Cl_6$, which was also structurally examined. Although **8**·4$CHB_{11}H_5Cl_6$ could not be obtained in a pure state as desired, during the recrystallization process, crystals with shapes different from those of **8**·4$CHB_{11}H_5Cl_6$ also fortuitously crystallized out, and they were determined to be pure samples of **13**·3$CHB_{11}H_5Cl_6$. The parent ion peak of **13** was observed at m/z 492.2300, which is in good agreement with the peak expected for trication $C_{100}H_{92}N_4O_8^{3+}$ (calculated value: 492.2300) using HR-ESI-MS. The ^{1}H NMR spectrum was silent, suggesting the existence of an unpaired electron in the molecule. However, single crystals suitable for crystallographic measurements could not be obtained.

As for **8**, the presence of four counteranions per molecule implied that the cationic organic moiety was a tetracation. The two connected acridinium units were found to form a highly coplanar structure with the dihedral angles of the two acridinium units being 0.2(1)° (X = $SbCl_4^-$) and 2.0(1)° (X = $CHB_{11}H_5Cl_6^-$), and the sum of the bond angles around nitrogen being 360.1(4)° (X = $SbCl_4^-$) and 359.9(3)° (X = $CHB_{11}H_5Cl_6^-$). The bond lengths between the two acridinium cation moieties were C2−C2* = 1.42(1) Å (X = $SbCl_4^-$) and 1.419(6) Å (X = $CHB_{11}H_5Cl_6^-$), and were longer than that of a typical double bond (1.34 Å), but shorter than that of a typical biphenyl single bond (1.48 Å). This suggests the contribution of both the quinoidal form **8A** with closed-shell structure and the nonquinoidal form **8B** with singlet diradical character, as shown in Figure 1. A similar phenomenon was also observed in the case of Chichibabin's hydrocarbon[20] (Figure 2) in which the bond connecting the two phenylene moieties (1.448(4) Å) was also longer than a typical double bond. This interesting X-ray structure of **8** prompted us to study its singlet diradical character in more detail.

2.3. Evaluation of the Singlet Diradical Character of Isolated Dimer 8 Based upon X-ray Structure and Computational Analysis. To establish a better understanding of the ground state of dimer **8**, single-point calculations of its singlet and triplet states were performed at the BHandHLYP/6-31G(d) level. The molecular geometry of dimer **8**·4$SbCl_4$ obtained from X-ray diffraction data was used excluding the counteranions and incorporated solvent molecules. Surprisingly, the most stable electronic state is that of the open-shell singlet (OS), according to calculations by the broken-symmetry (BS) DFT method. The closed-shell singlet (CS) solution obtained by the spin-restricted DFT method is higher in energy than the OS solution corrected by the approximate spin-projection (AP) method[27] using both the open- and the closed-shell solutions ($\Delta E^{AP}_{OS\text{-}CS}$ = −13.7 kcal/mol). The energy of the triplet state is also higher than that of the OS solution corrected by the AP method ($\Delta E^{AP}_{OS\text{-}T}$ = −8.9 kcal/mol). The diradical character y of the dimer, estimated by the occupancy of the lowest unoccupied natural orbital (LUNO) at the BHandHLYP/6-31G(d) level, is 0.615, indicating that the species has intermediate character between a pure singlet diradical and a closed-shell species.[12] The spin density distribution in the open-shell singlet was also calculated at the UBHandHLYP/6-31G(d) level (Figure 5), and it was

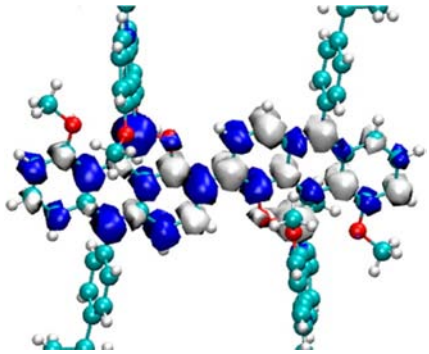

Figure 5. The full spin density distribution of **8** in the open-shell singlet state. Only the central part of the structure, where the distribution is concentrated, is shown. The calculations were performed at the UBHandHLYP/6-31G(d) level of theory. Spin densities are drawn at the 0.002 au threshold level.

Table 1. Selected Bond Lengths (Å) for Tetracation Dimer 8·4SbCl$_4$ from Its X-ray Structure and for the Optimized Structure of Tetracation Dimer 8 Calculated at the RB3LYP/6-31G(d) and UB3LYP/6-31G(d) Levels of Theory

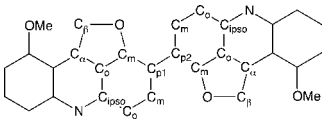

	N−C$_{ipso}$/Å	C$_{p1}$−C$_{p2}$/Å	C$_\alpha$−C$_\beta$/Å	avg C$_{ipso}$−C$_o$ and C$_m$−C$_p$/Å	avg C$_o$−C$_m$ /Å	bond length difference[a]
X-ray structure[b]	1.336(10)	1.42(1)	1.374(2)	1.417(12)	1.373(10)	0.044(22)
closed-shell singlet[b,c]	1.352	1.428	1.394	1.429	1.377	0.052
open-shell singlet[b,d]	1.363	1.451	1.402	1.420	1.384	0.036
triplet[b,d]	1.374	1.474	1.410	1.412	1.390	0.022

[a]Difference between the average of all C$_{ipso}$−C$_o$ and C$_m$−C$_p$ bond lengths and the average of C$_o$−C$_m$ bond lengths. [b]Bond lengths are the average of corresponding bonds of the two acridinium moieties. [c]Calculated at the B3LYP/6-31G(d) level. [d]Calculated at the UB3LYP/6-31G(d) level.

found that the largest spin densities are observed on the carbon atoms connecting the planar dimeric core to the peripheral acridinium substituents (formerly the allenic carbon atoms of the precursor) and the nitrogen atoms. Thus, this species is best described as a ca. 1:1 resonance hybrid of quinoidal structure **8A** and diradical structure **8B**.

The open-shell character of tetracation dimer **8** was further examined from the viewpoint of geometric structure. Geometry optimizations of tetracation dimer **8** were performed at the RB3LYP/6-31G(d) level for the singlet state, and at the UB3LYP/6-31G(d) level for the BS singlet and triplet states. The y value of the BS singlet structure (optimized at the UB3LYP/6-31G(d) level) is 0.685 (at the UBHandHLYP/6-31G(d) level), which is consistent with the LUNO occupation of 0.615 calculated at the UBHandHLYP level on the full structure based on X-ray analysis. The average bond lengths of selected bonds and average bond length differences for alternating bonds are summarized in Table 1 (see the Supporting Information for details). The electronic structure of **8** can be described by the resonance between the quinoidal form **8A** with bond alternation (closed-shell) and the nonquinoidal form **8B** with pure singlet diradical character. We therefore focused on the bond length alternations of the benzene ring fused to a furan ring in the quinoidal form **8A**, that is, C$_o$−C$_m$ versus C$_{ipso}$−C$_o$ and C$_m$−C$_p$. The differences in the averages of these bonds, that is, 0.044(22) Å (the X-ray structure) and 0.036 Å (the optimized open-shell singlet structure), are found to lie between those for the optimized closed-shell (0.052 Å) and pure diradical triplet (0.022 Å) structures, suggesting an intermediate diradical character in the singlet ground state of **8**.

To obtain more evidence for the singlet diradical nature of the tetracation dimer, SQUID measurements of **8**·4CHB$_{11}$H$_5$Cl$_6$ were carried out. For singlet diradical species, the excited triplet state is generally accessible, and this transition process is observed as an increase in the population of the magnetized state upon increase of temperature. Thus, observations of such transitions in SQUID measurements can be considered as indications of the presence of the open-shell singlet ground state. However, in the case of **8**, the excited triplet species could not be observed (see the Supporting Information). This could be due in part to the population of the open-shell singlet diradical state, which was only about one-half, and to a larger extent to the presence of a large singlet−triplet gap as estimated by AP calculations of **8**, in addition to the inevitable intrinsic error associated with the measurement.

2.4. Redox Reactions of Dimer Species. To obtain a deeper understanding of the electronic nature of the dimer species, redox reactions of the dimer were investigated. Treatment of tetracation dimer **8**·4SbCl$_4$ with excess Zn metal afforded dication dimer **12**·2SbCl$_4$ in 80% yield (Scheme 4). After counteranion exchange of SbCl$_4^-$ for TfO$^-$, the product, **12**·2OTf, was treated with an excess amount of AgOTf, and it was found that the tetracation dimer was regenerated in the form of **8**·4OTf in 78% isolated yield. It is especially noteworthy that **8**·4OTf obtained by this method was free of **13** as an impurity, in contrast to the product of the oxidation reaction of **3b**. A CD$_2$Cl$_2$ solution of **8**·4OTf in the presence of excess AgOTf, which was used to guarantee suppression of the formation of **13**, still showed a partially broadened ^{1}H NMR spectrum at room temperature, suggesting the existence of unpaired electrons (Figure 6). When the excess AgOTf was removed, radical impurity **13** gradually formed.

Scheme 4. Redox Reaction of the Dimer Species

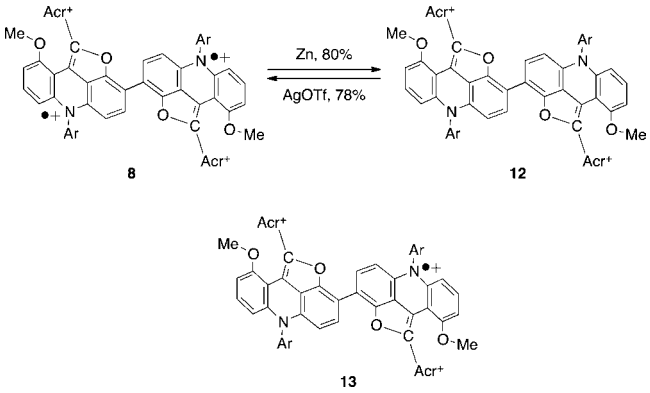

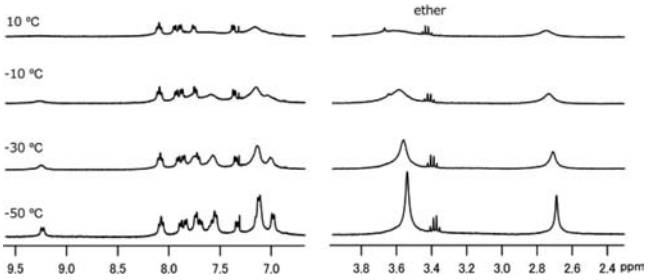

Figure 6. VT ^{1}H NMR of dimer **8**·4OTf in the presence of excess AgOTf in CD$_2$Cl$_2$. The aromatic region is given on the left, and the signals of the methyl groups observed at 2.69 (6H) and 3.54 (12H) ppm are shown on the right.

Thus, we could not use pure **8** for TPA experiments in section 2.8. The ^{1}H NMR spectra of singlet diradical species are known to become broad due to the accessibility of the excited triplet state at higher temperatures. Because there was a possibility that this phenomenon was operative for our compound, we carried out variable temperature (VT) NMR measurements. By cooling the temperature to −50 °C, the ^{1}H NMR spectrum in CD_2Cl_2 became sharper. At present, we cannot leave out other factors that might lead to this NMR behavior, but it is likely that the reason stems from the singlet diradical origin of the species. This is consistent with the singlet-to-triplet ratio (∼3 × 10^6) of the excited triplet at room temperature estimated from the calculated value of $\Delta E^{AP}_{OS\text{-}T}$ = −8.9 kcal/mol mentioned in the previous section.

2.5. Plausible Reaction Mechanism. Next, stepwise oxidation of allene **3b** was carried out to reveal the reaction mechanism (Scheme 5). The oxidation of allene **3b** with 1 equiv of $(4\text{-}BrC_6H_4)_3N^{\bullet+}SbCl_6^-$ gave demethylated monomer **14**·$SbCl_6$ as confirmed by ESI−MS and ^{1}H NMR. The parent ion peak of **14**·$SbCl_6$ was observed at m/z 739.3518 (calcd for $C_{50}H_{47}O_4N_2^+$: 739.3530) using HR-ESI−MS. The identity of the counteranion was confirmed with the negative mode. The ^{1}H NMR spectrum of **14**·$SbCl_6$ in $CDCl_3$ showed two Me groups at δ 2.74 (3H) and 3.64 (6H), and two *t*-Bu groups at δ 1.45 (9H) and 1.51 (9H), indicating the unsymmetrical nature of the structure of **14**·$SbCl_6$. These results suggest that **14**·$SbCl_6$ was formed by one-electron oxidation of **3b**. This would imply the elimination of a methyl radical from the initial intermediate formed upon electron removal from **3b**. However, because we do not have definite proof of the quantitative formation of **14**·$SbCl_6$, we cannot dismiss the possibility of a second oxidation by counteranion $SbCl_6^-$ to give an oxonium intermediate that could easily extrude the methyl group upon nucleophilic attack by a free chloride ion or a chlorine atom of $SbCl_6^-$, which is known as a source of nucleophilic chloride anions.[28] This corresponds to the mechanism previously assumed for the dimethoxythioxanthene system.[29] $SbCl_6^-$ is known to oxidize ferrocene, I^-[1], and aromatic amines; therefore, this assumption is not without reason.[30] This type of oxidation reaction would give rise to counteranions such as $SbCl_4^-$ and $Sb_2Cl_8^{2-}$, as observed here for **8**·4$SbCl_4$.[30]

For the second oxidation step, **14**·$SbCl_6$ was treated with 1 equiv of $(4\text{-}BrC_6H)_3N^{\bullet+}SbCl_6^-$ to afford trication monoradical species **13**, whose identity was verified by UV−vis−NIR measurements. Although tetracation species **8** was not included in crude product at all, these results suggest that the dimerization took place through demethylated intermediate **14**·$SbCl_6$. The formation of conjugated product **8** probably takes place in a manner similar to the formation of biaryls by oxidative coupling in general, which is facilitated by the presence of electron-donating oxygen substituents.[31] It should be noted that the initial target, triplet carbene **4b**, does not seem to be involved in this reaction.

Scheme 5. Plausible Reaction Mechanism

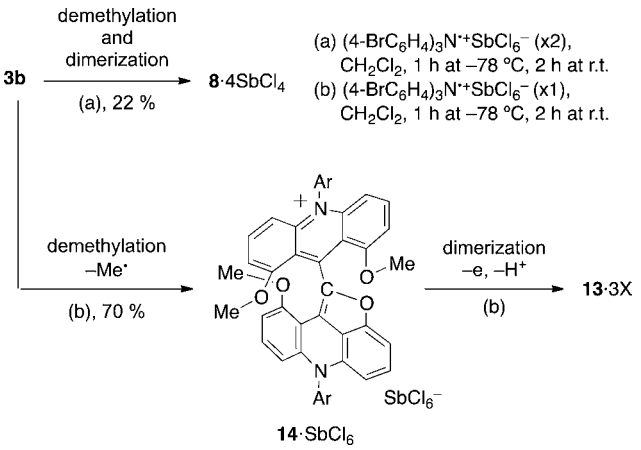

2.6. One-Photon Absorption (OPA) Spectra of Dimeric Species. Figure 7 shows the OPA spectrum of **8**·4OTf in CH_2Cl_2. This spectrum of **8** also shows absorption by trication monoradical **13** (Scheme 4) because it was difficult to completely remove **13** from the product of the oxidation of allenic precursor **3**. In contrast, pure **13** was obtained during the recrystallization of **8**·4$CHB_{11}H_5Cl_6$, and the OPA spectrum is also shown in Figure 7. The OPA spectrum of **13**·3$CHB_{11}H_5Cl_6$ has broad and intense peaks in the near-infrared region (1449 and 1804 nm). These peaks originate from transitions involving a singly occupied molecular orbital (SOMO). Such near-infrared absorptions of radical ions were previously observed in some aromatic compounds and have been assigned to the SOMO → LUMO and HOMO → SOMO excitations.[32]

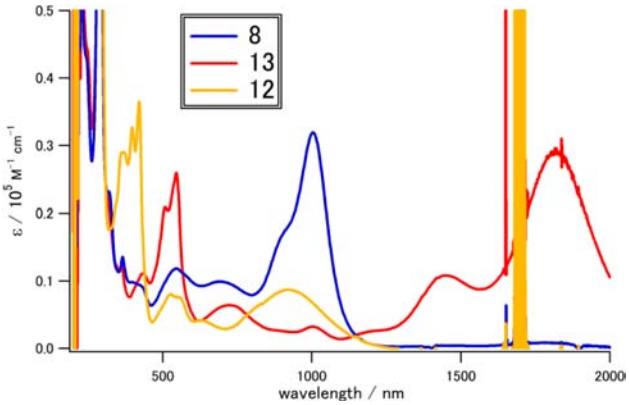

Figure 7. One-photon absorption spectra of dimers **8**·4OTf, **12**·2OTf, and **13**·3$CHB_{11}H_5Cl_6$ in CH_2Cl_2.

Besides the near-infrared absorption peaks of the residual **13**, the intense peak at 1000 nm and the shoulder at 900 nm in the spectrum for **8** in Figure 7 are attributed to inherent absorption of tetracation diradical **8**. Time-dependent DFT calculations at the UB3LYP/6-31G(d) level based on the geometry from X-ray analysis support that dimer **8** has two electron transitions in the near-infrared region (982.1 nm, oscillator strength f = 0.1001, HOMO−7 → LUMO and 1221 nm, f = 0.0964, HOMO → LUMO). Thus, the shoulder and the peak are reasonably assigned to HOMO−7 → LUMO and HOMO → LUMO transitions, respectively. The HOMO and LUMO are mainly localized in the two central acridine units that form the diradicaloid backbone structure (Figure 8), like in Chichibabin's hydrocarbon (Figure 2). Moreover, the small HOMO−LUMO gaps are a typical feature for high singlet diradical character in the ground state. Thus, these calculation results also support the conclusion that the ground state of **8** has singlet diradical character.

To ascertain the absorption spectrum of **8** more definitely, we also measured the reflection spectrum on the (111) face for

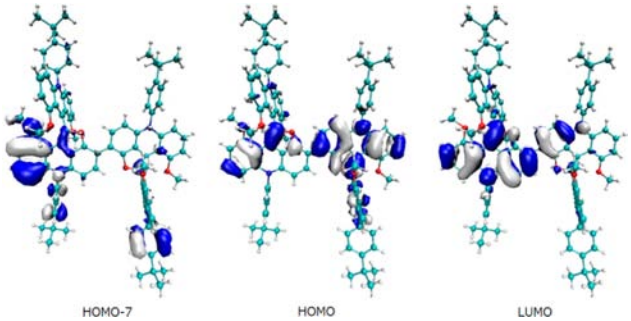

Figure 8. Shapes of the α molecular orbitals of **8** calculated at the UB3LYP/6-31G(d) level. The shapes are drawn at the 0.02 au threshold level.

a single crystal of pure **8**·4$SbCl_4$ with the polarization of light parallel to the *c*-axis. Kramers−Kronig transformation of the reflection spectrum gave the absorption spectrum of **8**·4$SbCl_4$ shown in Figure 9. The intense peaks at 952 and 1052 nm of

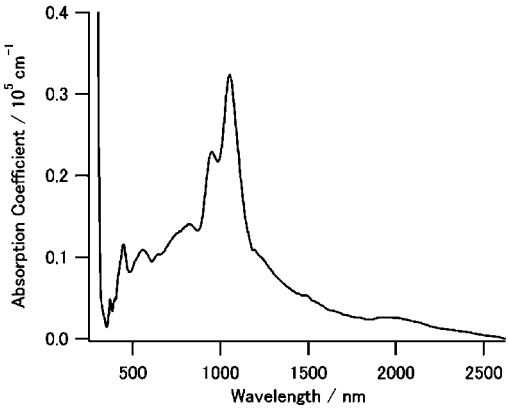

Figure 9. The absorption spectrum of a single crystal of **8**·4$SbCl_4$ obtained by Kramers−Kronig transformation of the reflection spectrum.

the obtained spectrum show good agreement with the near-infrared peaks in CH_2Cl_2, demonstrating that absorption peaks at 900 and 1000 nm in the spectrum of the solution sample definitely originate from **8**.

2.7. Diradical Character Dependence of Static Second Hyperpolarizabilities (γ) of Model Species. Before proceeding with TPA measurements, we theoretically examined the impact of diradical character on the static γ for the dimeric species. To focus on the diradical character effects in tetracation dimer **8**, we considered a simplified model (**8′**) composed of two central acridines that form a diradicaloid backbone structure. In the model, Acr^+, OMe, and Ar of **8** are replaced by hydrogen atoms; thus, the system is a dication. From geometry optimization at the UB3LYP/6-31G(d) level, we obtained a planar structure. Both diradical character (y = 0.605) and spin density distribution of **8′** calculated at the UBHandHLYP/6-31G(d) level are found to be very close to those of original tetracation dimer **8** (see Figures 5 and 10a). We also considered a two-electron reduced model (**12′**) of **8′**, which corresponds to closed-shell dication dimer **12**. The optimized structure of **12′** was found to be slightly nonplanar, neutral, and closed shell (y = 0). As a result, these models are expected to be useful for our purposes.

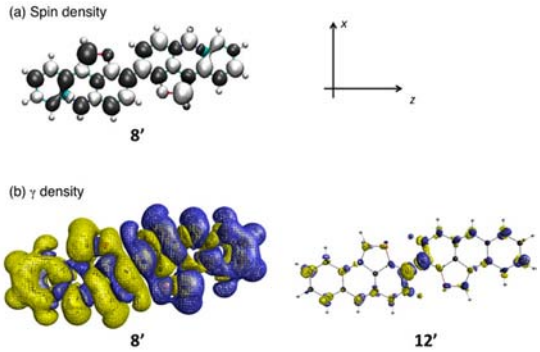

Figure 10. Spin density distribution of **8′** (a), and γ density distributions (b) of **8′** (open-shell singlet) and **12′** (closed-shell species). These densities are drawn at threshold values of 0.002 au for (a) and 500 au for (b). Yellow and blue meshes in the γ density plots represent the positive and negative regions, respectively.

Static γ values were calculated by the finite-field method using the total energies under the static electric field obtained at the U(R)BHandHLYP/6-31G(d) level of approximation (for details, see the Supporting Information). The results of the calculations are summarized in Table 2. The *z*-axis component

Table 2. Diradical Character *y* and *z*-Axis Component of Static γ (γ_{zzzz}) of Model Dimeric Species 8′ and 12′ Calculated at the U(R)BHandHLYP/6-31G(d) Level

compound	y	$\gamma_{zzzz}/10^3$ au
8′ (dication)	0.605	3100
12′ (neutral)	0.0	217

of static γ of diradical species **8′** (3100×10^3 au) was found to be more than 10 times as large as that of closed-shell counterpart **12′** (217×10^3 au). Such significant enhancement of static γ in the diradical species supports our theoretical prediction.[9c] Further, the amplitude of the γ value of **8′** is on the same order as those of bis(phenalenyl) compounds that have already been found to exhibit significant TPA cross sections.[11a,14]

To further clarify the spatial contributions of electrons to the enhancement of γ in diradical species **8′**, we applied γ density analysis.[22] The γ density represents the field-induced response of charge density proportional to the cubic of the external electric field amplitude. Positive and negative γ densities represent the increase and decrease of charge densities related to the third-order polarization, respectively. The sign of the contribution to γ is positive when the direction from positive to negative γ density coincides with the positive direction on the coordinate axis, and the sign becomes negative in the opposite case. The magnitude of the contribution associated with this pair of γ densities is proportional to the distance between them. The γ density distributions of these models are shown in Figure 10b. For open-shell species **8′**, large positive (yellow) and negative (blue) γ densities, dominated by π electrons, are found to be well separated at the left- and right-hand sides of the system, leading to significant positive contributions to γ. The region with large positive and negative γ densities is found to be well correlated to that with primary spin densities, the feature of which indicates strong impact of diradical character on γ enhancement. In sharp contrast, the γ density amplitudes of closed-shell species **12′** are found to be negligible in the whole region of the system. These results substantiate the significant

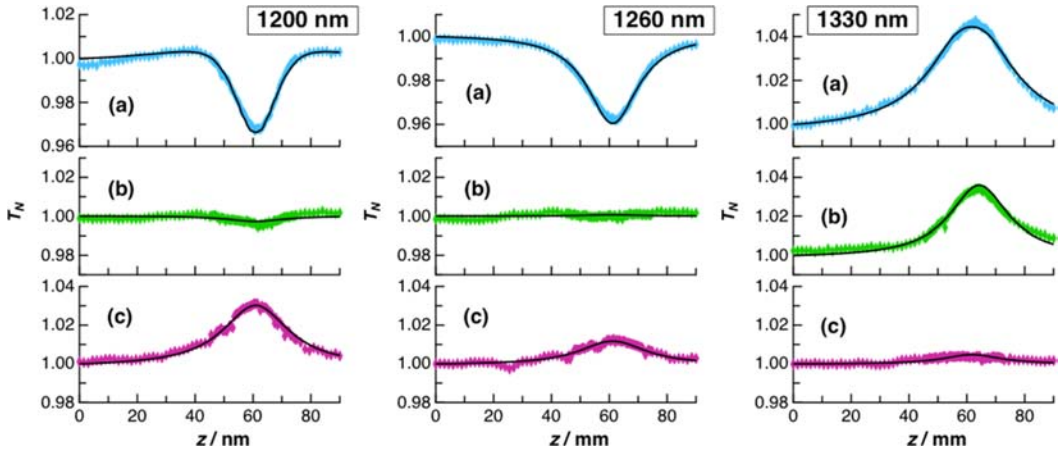

Figure 11. Open-aperture Z-scan traces (normalized transmittance T_N versus the sample position z) of impure **8**·4SbCl$_4$ (a), **13**·3CHB$_{11}$H$_5$Cl$_6$ (b), and **12**·2SbCl$_4$ (c) at wavelengths of 1200 nm (left), 1260 nm (middle), and 1330 nm (right). Solid curves are theoretical fits (see the Supporting Information) to the recorded data (symbols). All samples are in CH$_2$Cl$_2$.

Table 3. Diradical Character y and Two-Photon Absorption Cross Section $\sigma^{(2)}$ of Dimeric Species 8, 12, and 13 at Different Wavelengths

		$\sigma^{(2)}$/GM[b]				
compound	y[a]	1200 nm	1230 nm	1260 nm	1300 nm	1330 nm
8[c]	0.685	3560 ± 410	2350 ± 300	1590 ± 250	455 ± 66	396 ± 52
12	0.000	<9	<21	<11	0	0
13	–[d]	<140	<110	<73	0	0

[a]Calculated at the UBHandHLYP/6-31G(d) level. The structures were optimized by UB3LYP/6-31G(d). [b]1 GM = 10^{-50} cm^4 s molecule^{-1} photon^{-1}. [c]Contribution of resulting **13** was subtracted for (2) (see the Supporting Information). [d]Indefinable for monoradical species.

difference in γ amplitudes between **8′** and **12′** (see Table 2). From these results, open-shell tetracation dimer **8** is expected to exhibit significantly large TPA cross sections as compared to closed-shell dicationic counterpart **12**.

2.8. Two-Photon Absorption (TPA) Measurements of Dimeric Species. Following the results shown in previous sections that tetracation dimer **8** has relatively high singlet diradical character, TPA measurements of **8**·4SbCl$_4$, closed-shell dication **12**, and monoradical trication **13** were performed by the open-aperture Z-scan method to clarify the relationship between diradical character and TPA properties. The samples for this study were prepared by dissolving the compounds in CH$_2$Cl$_2$. Although we had pure samples of **12**·2SbCl$_4$ and **13**·3CHB$_{11}$H$_5$Cl$_6$, the available sample of **8**·4SbCl$_4$ contained residual **13** due to the difficulty of the separation (as mentioned in previous sections). Therefore, we conducted measurements for the impure sample of **8** and separated the contribution of **8** from the impure solution by comparing the results to those obtained for the solution of pure **13**.

For the measurements, the excitation wavelength was scanned from 1200 to 1300 nm, where the OPAs of the samples are relatively small (Figure 7). Panels in the top row in Figure 11 show typical Z-scan traces of the solution of impure **8**. At 1260 nm, a clear concave curve centered at the focal point (z = 61 mm) was observed (the top-middle panel), indicating that strong TPA occurs at this wavelength. The opposite shape, that is, a convex transmittance curve centered at the focal point, was also observed at the longest wavelength (1330 nm, top-right). This convex curve means that the OPA of the sample at this wavelength decreased with increasing optical intensity by the saturable absorption (SA) process. At the shortest wavelength (1200 nm, top-left), the intermediate case was observed; the Z-scan trace showed an "M"-like shape, that is, a concave curve overlapping a broad convex curve, suggesting that TPA overlaps SA.

As pure **13** (the middle row in Figure 11) gave almost no signal at the wavelengths of 1200 and 1260 nm, it can be concluded that the strong TPA observed for impure **8** at these wavelengths originates from **8** rather than **13**. Meanwhile, a strong SA signal was also observed for pure **13** at 1330 nm (the middle-right), which can also contribute to the SA signal observed for **8** at the same wavelength. Here, we ignore the difference in counteranions, which are SbCl$_4^-$ for the impure **8**; thus, the residual signals were from **13**·3SbCl$_4$ for **8**, and CHB$_{11}$H$_5$Cl$_6^-$ for the pure **13**. This simplification is reasonably justified because the OPA spectra of **13** with different counteranions were almost the same, except for minor spectral shifts (the near-infrared peaks were 1461 and 1823 nm for the impure solution with the counteranion of SbCl$_4^-$, and 1444 and 1826 nm for pure **13**·3CHB$_{11}$H$_5$Cl$_6$), suggesting that the choice of counteranion does not have a significant influence on the electronic states of **13**. In comparison to **8** and **13**, closed-shell species **12** gave rather simple Z-scan traces (the bottom row in Figure 11). The magnitudes of the SA signals in the recorded traces always decreased as the wavelength increased and had no indication of TPA.

Quantitative analysis of the recorded Z-scan traces was performed by using the curve-fitting procedure with the theoretical model assuming spatial and temporal Gaussian profiles for the incident laser pulses (see the Supporting Information). The observed traces were well reproduced with the fitting curves (solid curves in Figure 11). In the procedure to calculate the TPA cross section $\sigma^{(2)}$, we estimated the concentration of **13** in the impure sample from the one-photon

absorption spectrum and then subtracted its contribution from the total $\alpha^{(2)}$ of the impure solution; however, the contribution of **13** was found to be negligible as compared to that of **8**.[33] The TPA cross sections obtained for each dimeric species are listed in Table 3. Clearly, diradical dimer **8** has much larger $\sigma^{(2)}$ than the other species at each wavelength. The maximum value was $\sigma^{(2)}$ = 3560 ± 410 GM at 1200 nm, which is a relatively large value for an organic chromophore. The resonance enhancement by the HOMO → LUMO transition of OPA may be involved in the large $\sigma^{(2)}$. In contrast, closed-shell singlet **12** did not show any notable TPA; the $\sigma^{(2)}$ values are at least 2 orders of magnitude smaller than those of diradical dimer **8**. This is the first direct comparison, to the best of our knowledge, between a singlet diradicaloid (**8**, y = 0.682) and its closed-shell counterpart (**12**, y = 0.000), which have the same backbone structure and atom composition, although comparisons between molecules having similar π-conjugation (but different backbones or atom compositions) have been previously demonstrated.[13,14,21] These results support our theoretical prediction that molecules having intermediate diradical character have large third-order nonlinearity including TPA.[9,11]

3. CONCLUSIONS

In summary, during our attempts to synthesize stable triplet carbenes, a dimeric product **8** having singlet diradical nature in the ground state was serendipitously obtained upon the oxidation of an allenic precursor (**3**) bearing 1,8-dimethoxyacridine moieties using 2 equiv of $(4\text{-BrC}_6\text{H}_4)_3\text{N}^{\bullet+}\text{SbCl}_6^-$. The diradical nature of **8** in the ground state was supported by X-ray structural analysis and DFT calculations. Furthermore, the corresponding dicationic dimer **12** was furnished upon treatment of tetracation dimer **8** with Zn. Trication **13** was also obtained as a byproduct of the oxidation of allenic precursor **3**. These three dimeric species, which have the same structural backbone and atom composition, but different spin states, enabled us to directly compare the dependence of TPA properties on different diradical characters to test the theoretical prediction that a molecule with intermediate diradical character ($0 < y < 1$) has larger optical nonlinearity than the corresponding closed-shell electronic structure (y = 0).[9,11] Two-photon absorption measurements of the three species showed significant differences depending on singlet diradical character y. This is the first straightforward demonstration supporting the theoretical prediction because the same molecular backbone and atom composition are retained across the compared species. Together with the previous studies,[13,14,21] the present results clearly show that singlet diradical character with intermediate magnitude can be a new molecular parameter for excellent TPA materials in the near-infrared region. Moreover, it can be pointed out that the present results suggest the possibility of switching the TPA magnitude by using redox reactions, as reported for condensed-ring fluorene derivatives.[34] The use of redox reactions to switch TPA properties may open new possibilities such as highly sensitive detection of intermediate species of such reactions.

■ ASSOCIATED CONTENT

Ⓢ Supporting Information

Synthetic, experimental, and calculation procedures, characterization data including crystallographic measurements, geometry optimizations of tetracation dimer **8**, SQUID data mentioned in section 2.3, and additional details related to the curve fitting procedures and analysis of the TPA measurements for an impure sample of **8** mentioned in section 2.7. This material is available free of charge via the Internet at http://pubs.acs.org.

■ AUTHOR INFORMATION

Corresponding Author

k.kamada@aist.go.jp; yyama@sci.hiroshima-u.ac.jp

Present Address

⊥Research Institute of Instrumentation Frontier, National Institute of Advanced Industrial Science and Technology (AIST), Tsukuba, Ibaraki 305-8565, Japan.

Notes

The authors declare no competing financial interest.

■ ACKNOWLEDGMENTS

This work was supported by two Grants-in-Aid for Scientific Research on Priority Areas (nos. 14340199 and 17350021) from the Ministry of Education, Culture, Sports, Science and Technology, Japan. This work was also supported by a Grant-in-Aid for Scientific Research (no. 21350011) from the Japan Society for the Promotion of Science (JSPS). We are thankful to the Natural Science Center for Basic Research and Development (N-BARD), Hiroshima University, for combustion analysis measurements on some of the new compounds. We acknowledge the Research Center for Computational Science, Okazaki, Japan, for machine time on their computer system. We also thank Assistant Prof. Eigo Miyazaki and Prof. Kazuo Takimiya of the Department of Applied Chemistry, Graduate School of Engineering, Hiroshima University, for UV−vis−NIR measurements and Prof. Manabu Abe of the Department of Chemistry, Graduate School of Science, Hiroshima University, for ESR measurements.

■ REFERENCES

(1) Salem, L.; Rowland, C. *Angew. Chem., Int. Ed. Engl.* **1972**, *11*, 92−111.

(2) (a) Lambert, C. *Angew. Chem., Int. Ed.* **2011**, *50*, 1756−1758. (b) Sun, Z.; Wu, J. *J. Mater. Chem.* **2012**, *22*, 4151−4160.

(3) Bendikov, M.; Duong, H. M.; Starkey, K.; Houk, K. N.; Carter, E. A.; Wudl, F. *J. Am. Chem. Soc.* **2004**, *126*, 7416−7417.

(4) Bettinger, H. F. *Pure Appl. Chem.* **2010**, *82*, 905−915.

(5) (a) Tonshoff, C.; Bettinger, H. F. *Angew. Chem., Int. Ed.* **2010**, *49*, 4125−4128. (b) Purushothaman, B.; Bruzek, M.; Parkin, S. R.; Miller, A.-F.; Anthony, J. E. *Angew. Chem., Int. Ed.* **2011**, *50*, 7013−7017.

(6) (a) Kubo, T.; Shimizu, A.; Sakamoto, M.; Uruichi, M.; Yakushi, K.; Nakano, M.; Shimoi, D.; Sato, K.; Takui, T.; Morita, Y.; Nakatsuji, K. *Angew. Chem., Int. Ed.* **2005**, *44*, 6564−6568. (b) Shimizu, A.; Uruichi, M.; Yakushi, K.; Matsuzaki, H.; Okamoto, H.; Nakano, M.; Hirao, Y.; Matsumoto, K.; Kurata, H.; Kubo, T. *Angew. Chem., Int. Ed.* **2009**, *48*, 5482−5486.

(7) Huang, J.; Kertesz, M. *J. Am. Chem. Soc.* **2007**, *129*, 1634−1643.

(8) Nakano, M.; Nagao, H.; Yamaguchi, K. *Phys. Rev. A* **1997**, *55*, 1503−1513.

(9) (a) Nakano, M.; Kishi, R.; Nitta, T.; Kubo, T.; Nakasuji, K.; Kamada, K.; Ohta, K.; Champagne, B.; Botek, E.; Yamaguchi, K. *J. Phys. Chem. A* **2005**, *109*, 885−891. (b) Nakano, M.; Kishi, R.; Ohta, S.; Takebe, A.; Takahashi, H.; Furukawa, S.; Kubo, T.; Morita, Y.; Nakasuji, K.; Yamaguchi, K.; Kamada, K.; Ohta, K.; Champagne, B.; Botek, E. *J. Chem. Phys.* **2006**, *125*, 074113. (c) Nakano, M.; Kishi, R.; Ohta, S.; Takahashi, H.; Kubo, T.; Kamada, K.; Ohta, K.; Botek, E.; Champagne, B. *Phys. Rev. Lett.* **2007**, *99*, 033001. (d) Nakano, M.; Yoneda, K.; Kishi, R.; Takahashi, T.; Kubo, T.; Kamada, K.; Ohta, K.; Botek, E.; Champagne, B. *J. Chem. Phys.* **2009**, *131*, 114316.

(10) (a) He, G. S.; Tan, L.-S.; Zheng, Q.; Prasad, P. N. *Chem. Rev.* **2008**, *108*, 1245−330. (b) Pawlicki, M.; Collins, H. A.; Denning, R. G.; Anderson, H. L. *Angew. Chem., Int. Ed.* **2009**, *48*, 3244−3266.
(11) (a) Nakano, M.; Kubo, T.; Kamada, K.; Ohta, K.; Kishi, R.; Ohta, S.; Nakagawa, N.; Takahashi, H.; Furukawa, S.; Morita, Y.; Nakasuji, K. *Chem. Phys. Lett.* **2006**, *418*, 142−147. (b) Nakano, M.; Nagai, H.; Fukui, H.; Yoneda, K.; Kishi, R.; Takahashi, H.; Shimizu, A.; Kubo, T.; Kamada, K.; Ohta, K.; Champagne, B.; Botek, E. *Chem. Phys. Lett.* **2008**, *467*, 120−125. (c) Fukui, H.; Nakano, M.; Shigeta, Y.; Champagne, B. *J. Phys. Chem. Lett.* **2011**, *2*, 2063−2066.
(12) (a) Yamaguchi, K. Instability in Chemical Bonds. In *Self-Consistent Field. Theory and Applications*; Carbo, R., Klobukowski, M., Eds.; Elsevier: Amsterdam, 1990; pp 727−823. (b) Nakano, M.; Fukui, H.; Minami, T.; Yoneda, K.; Shigeta, Y.; Kishi, R.; Champagne, B.; Botek, E.; Kubo, T.; Ohta, K.; Kamada, K. *Theor. Chem. Acc.* **2011**, *130*, 711−724; **2011**, *130*, 725 (erratum).
(13) Kamada, K.; Ohta, K.; Shimizu, A.; Kubo, T.; Kishi, R.; Takahashi, H.; Botek, E.; Champagne, B.; Nakano, M. *J. Phys. Chem. Lett.* **2010**, *1*, 937−940.
(14) Kamada, K.; Ohta, K.; Kubo, T.; Shimizu, A.; Morita, Y.; Nakasuji, K.; Kishi, R.; Ohta, S.; Furukawa, S.; Takahashi, H.; Nakano, M. *Angew. Chem., Int. Ed.* **2007**, *46*, 3544−3546.
(15) (a) Hirai, K.; Tomioka, H. *J. Am. Chem. Soc.* **1999**, *121*, 10213−10214. (b) Itoh, T.; Nakata, Y.; Hirai, K.; Tomioka, H. *J. Am. Chem. Soc.* **2006**, *128*, 957−967.
(16) Iwamoto, E.; Hirai, K.; Tomioka, H. *J. Am. Chem. Soc.* **2003**, *125*, 14664−14665.
(17) Kawano, M.; Hirai, K.; Tomioka, H.; Ohashi, Y. *J. Am. Chem. Soc.* **2007**, *129*, 2383−2391.
(18) For the formation of cation radical dimers by oxidation, see: (a) Oka, H. *Org. Lett.* **2010**, *12*, 448−451. (b) Terada, E.; Okamoto, T.; Kozaki, M.; Masaki, M. E.; Shiomi, D.; Sato, K.; Takui, T.; Okada, K. *J. Org. Chem.* **2005**, *70*, 10073−10081. (c) Zheng, S.; Barlow, S.; Risko, C.; Kinnibrugh, T. L.; Khrustalev, V. N.; Jones, S. C.; Antipin, M. Y.; Tucker, N. M.; Timofeeva, T. V.; Coropceanu, V.; Brédas, J.-L.; Marder, S. R. *J. Am. Chem. Soc.* **2006**, *128*, 1812−1817. (d) Nishinaga, T.; Tateno, M.; Fujii, M.; Fujita, W.; Takase, M.; Iyoda, M. *Org. Lett.* **2010**, *12*, 5374−5377. (e) Ito, A.; Urabe, M.; Tanaka, K. *Angew. Chem., Int. Ed.* **2003**, *42*, 921−924.
(19) (a) Errede, L. A.; Landrum, B. F. *J. Am. Chem. Soc.* **1957**, *79*, 4952−4955. (b) Montgomery, L. K.; Huffman, J. C.; Jurczak, E. A.; Gredze, M. P. *J. Am. Chem. Soc.* **1986**, *108*, 6004−6011. (c) Hiroto, S.; Furukawa, K.; Shinokubo, H.; Osuka, A. *J. Am. Chem. Soc.* **2006**, *128*, 12380−12381. (d) Ishida, M.; Karasawa, S.; Uno, H.; Tani, F.; Naruta, Y. *Angew. Chem., Int. Ed.* **2010**, *49*, 5906−5909. (e) Takahashi, T.; Matsuoka, K.; Takimiya, K.; Otsubo, T.; Aso, Y. *J. Am. Chem. Soc.* **2005**, *127*, 8928−8929. (f) Kikuchi, A.; Iwahori, F.; Abe, J. *J. Am. Chem. Soc.* **2004**, *126*, 6526−6527.
(20) Montgomery, L. K.; Huffman, J. C.; Jurczak, E. A.; Gredze, M. P. *J. Am. Chem. Soc.* **1986**, *108*, 6004−6011.
(21) Ishida, M.; Shin, J.-Y.; Lim, J. M.; Lee, B. S.; Yoon, M.-C.; Koide, T.; Sessler, J. L.; Osuka, A.; Kim, D. *J. Am. Chem. Soc.* **2011**, *133*, 15533−15544.
(22) Nakano, M.; Shigemoto, I.; Yamada, S.; Yamaguchi, K. *J. Chem. Phys.* **1995**, *103*, 4175−4191.
(23) Yano, T.; Yamaguchi, T.; Yamamoto, Y. *Chem. Lett.* **2009**, *38*, 794−795.
(24) Ali, M. H.; Buchwald, S. *J. Org. Chem.* **2001**, *66*, 2560−2565.
(25) (a) Mass, G.; Singer, B. *Z. Naturforsch.* **1984**, *39b*, 1399. (b) Mass, G.; Singer, B. *Z. Naturforsch.* **1985**, *40b*, 90.
(26) For the structure of dimeric $SbCl_4^-$, see: (a) Gerasimenko, A. V.; Polishchuk, A. V.; Volkova, L. M.; Karaseva, E. T.; Karasev, V. E. *Russ. J. Coord. Chem.* **2008**, *34*, 8−13. (b) Bott, S. G.; Brammer, L.; Connelly, N. G.; Green, M.; Orpen, A. G.; Paxton, J. F.; Schaverien, C. J.; Bristow, S.; Norman, N. C. *J. Chem. Soc., Dalton Trans.* **1990**, 1957−1969.
(27) (a) Yamaguchi, K.; Takahara, Y.; Fueno, T.; Houk, K. N. *Theor. Chim. Acta* **1988**, *73*, 337−364. (b) Yamanaka, S.; Okumura, M.; Nakano, M.; Yamaguchi, K. *J. Mol. Struct.* **1994**, *310*, 205−218.
(28) Stiddard, M. H. B.; Townsend, R. E. *J. Chem. Soc. A* **1969**, 2355−2357.
(29) (a) Yamaguchi, T.; Yamamoto, Y.; Kinoshita, D.; Akiba, K.; Zhang, Y.; Reed, C. A.; Hashizume, D.; Iwasaki, F. *J. Am. Chem. Soc.* **2008**, *130*, 6894−6895. (b) Yano, T.; Yamaguchi, T.; Yamamoto, Y. *Chem. Lett.* **2009**, *38*, 794−795.
(30) Cowell, G. W.; Ledwith, A.; White, A. C.; Woods, H. J. *J. Chem. Soc. B* **1970**, 227−231.
(31) Kovacic, P.; Jones, M. B. *Chem. Rev.* **1987**, *87*, 357−379.
(32) (a) Ohashi, K.; Kubo, T.; Masui, T.; Yamamoto, K.; Nakasuji, K.; Takui, T.; Kai, Y.; Murata, I. *J. Am. Chem. Soc.* **1998**, *120*, 2018−2027. (b) Angliker, H.; Gerson, F.; Lopez, J.; Wirz, J. *Chem. Phys. Lett.* **1981**, *81*, 242−246. (c) Angliker, H.; Rommel, E.; Wirz, J. *Chem. Phys. Lett.* **1982**, *87*, 208−212.
(33) See the Supporting Information.
(34) Cho, N.; Zhou, G.; Kamada, K.; Kim, R. H.; Ohta, K.; Jin, S.-H.; Müllen, K.; Lee, K.-S. *J. Mater. Chem.* **2012**, *22*, 185−191.